

## INFRARED SPACE OBSERVATORY PHOTOMETRIC SEARCH OF MAIN-SEQUENCE STARS FOR VEGA-TYPE SYSTEMS<sup>1</sup>

S. B. FAJARDO-ACOSTA,<sup>2,3</sup> R. E. STENCEL,<sup>2,4</sup> D. E. BACKMAN,<sup>5</sup> AND N. THAKUR<sup>2,6</sup>

Received 1999 September 1; accepted 1999 March 1

### ABSTRACT

We obtained 3.6–20  $\mu\text{m}$  photometry of 38 bright [*IRAS*  $F_{\nu}(12 \mu\text{m}) > 0.7 \text{ Jy}$ ] main-sequence stars with the *Infrared Space Observatory* (*ISO*). Observations were conducted with the ISOPHOT instrument, in the single-pointing photometry mode, through filters at 3.6, 11.5, and 20.0  $\mu\text{m}$ . We searched for excess (Vega-type) emission from dust at temperatures  $\gtrsim 100 \text{ K}$ , located at  $\sim 1$ –60 AU from the stars. We thus sampled dust at warm, terrestrial material temperatures and at cool ( $\sim 100 \text{ K}$ ) temperatures of possible Kuiper Belt-type regions in these systems. We detected 20  $\mu\text{m}$  excesses from  $\sim 14\%$  of our sources, but we did not detect 11.5  $\mu\text{m}$  excesses from any of them. We present single-temperature blackbody models of the location and density of dust emission around 10 stars, two of them (29 Cyg and Gl 816) with excesses newly reported here. We make a thorough comparison of *ISO* and *IRAS* data on our target stars and propose a new calibration procedure for ISOPHOT staring measurements at 3.6, 11.5, and 20  $\mu\text{m}$ .

*Subject headings:* circumstellar matter — dust, extinction — infrared: stars

### 1. INTRODUCTION

Photometry and spectroscopy of circumstellar dust in main-sequence stars are powerful tools with which to study extrasolar planetary material. A central question is how often main-sequence stars harbor these kinds of systems and how detectable they are. The *Infrared Space Observatory* (*ISO*; Kessler et al. 1996) offers an opportunity to answer these questions. *ISO* results will extend those from *IRAS*, particularly for main-sequence stars with only upper limits in *IRAS* data or for measurements with contaminating sources in the larger *IRAS* beam. Previous results from *IRAS* and *ISO* surveys of nearby field main-sequence stars (see the review by Backman & Paresce 1993, hereafter BP93; Plets 1997; Dominik & HJHVEGA Consortium 1998; Mannings & Barlow 1998) suggest that 15%–50% of these stars have circumstellar dust emitting in the far-infrared.

Observations of these systems in the far-infrared let us study dust at temperatures of  $\sim 50$ –125 K, located a few tens to a few hundred AU from the stars in the case of the A-star prototypes  $\alpha \text{ Lyr}$ ,  $\alpha \text{ PsA}$ , and  $\beta \text{ Pic}$  (BP93). These dust regions are therefore possible analogs in scale to the solar system’s Kuiper Belt (Tremaine 1990). Observations at mid-infrared wavelengths let us probe dust at approximately terrestrial material temperatures, within a few AU from the stars (Backman 1998). The disk of  $\beta \text{ Pic}$  contains a small amount of dust,  $\sim 5 \times 10^{-6} M_{\oplus}$ , at temperatures of  $\gtrsim 350 \text{ K}$ , within 30 AU from the star, detected via silicate spectroscopy (Knacke et al. 1993). *IRAS* and ground-based follow-up surveys (Aumann & Probst 1991) find that few main-sequence stars have warm dust ( $T > 150 \text{ K}$ ).

However, some systems have recently been studied via detailed photometry in the 10  $\mu\text{m}$  “silicate” filters, and warm dust ( $T \sim 220$ –340 K) has been detected at distances of  $\sim 4$ –12 AU from five stars (Fajardo-Acosta, Telesco, & Knacke 1998). This material, if resolved and mapped, could trace the dynamical effects of planets or protoplanets, as in the  $\beta \text{ Pic}$  disk (Lagage & Pantin 1994; Burrows et al. 1995; Heap et al. 1997).

In order to extend previous *IRAS* photometry surveys of main-sequence circumstellar dust, particularly at mid-infrared wavelengths, we observed main-sequence stars in what constituted an *ISO* Key Program (Stencel & Backman 1994). Here we report the results of our survey.

### 2. OBSERVATIONS AND DATA REDUCTION

We selected stars for our observations from the Yale Bright Star Catalog (Hoffleit & Jascheck 1982) of spectral types A to mid-G, and from the Gliese Catalog (Gliese 1969; Gliese & Jahreiss 1979) of spectral types mid-G to M. We also observed a few late-B stars. The selected stars had SIMBAD luminosity classifications of V, IV–V, or IV, and through the use of SIMBAD V (visual) magnitudes, spectral types, and ground-based trigonometric parallaxes (Jenkins 1963) we checked that the stars’ positions in the H-R diagram were no more than  $\sim 1 \text{ mag}$  above the zero-age main-sequence (ZAMS). We further chose only sources with color-corrected 12  $\mu\text{m}$  flux densities  $\geq 0.7 \text{ Jy}$  (or  $[12] \lesssim +4 \text{ mag}$ ) either from the *IRAS* Point Source Catalog Version 2 (Joint *IRAS* Science Working Group 1988, hereafter PSC), or from V magnitudes and predictions of  $V - [12]$  for normal stars (Waters, Coté, & Aumann 1987).

Our lower limit to the 12  $\mu\text{m}$  flux density translates into a volume-limited observing sample of stars. However, the corresponding upper limit to the distance depends on stellar spectral type. This limit is  $\sim 33 \text{ pc}$  for A5 V,  $\sim 19 \text{ pc}$  for F5 V,  $\sim 14 \text{ pc}$  for G5 V,  $\sim 9 \text{ pc}$  for K5 V, and  $\sim 3 \text{ pc}$  for M5 V, if the stars do not have any 12  $\mu\text{m}$  excess. Within these limiting distances we could choose only a fraction of the available stars from the Bright Star and Gliese catalogs, due to *ISO* observing time constraints. Some of the brightest main-sequence stars, such as  $\alpha \text{ Lyr}$ , have been observed in other *ISO* Key programs. We arbitrarily selected roughly

<sup>1</sup> Based on observations with *ISO*, an ESA project with instruments funded by ESA member states, with the participation of ISAS and NASA.

<sup>2</sup> University of Denver, Department of Physics and Astronomy, 2112 E. Wesley Avenue, Denver, CO 80208.

<sup>3</sup> Current address: IPAC, 770 S. Wilson Ave., Mail Stop 100-22, Pasadena, CA 91125; fajardo@ipac.caltech.edu.

<sup>4</sup> rstencel@phoenix.phys.du.edu

<sup>5</sup> Franklin and Marshall College, Physics and Astronomy Department, P.O. Box 3003, Lancaster, PA 17604-3003; d\_backman@acad.fandm.edu.

<sup>6</sup> nthakur@du.edu

equal numbers of stars of each spectral type from the above catalogs; the 38 selected stars are listed in Table 1. Our selected stars represent  $\sim 4.2\%$  of available A-type stars that satisfied our criteria in the above catalogs,  $\sim 2.4\%$  of F stars,  $\sim 4.4\%$  of G stars,  $\sim 4.4\%$  of K stars, and  $\sim 56\%$  of M stars. Overall, they represent  $\sim 5\%$  of V, IV–V, and IV stars in the Bright Star and Gliese catalogs brighter than 0.7 Jy at  $12\ \mu\text{m}$  and within  $\sim 1$  mag of the ZAMS.

We obtained photometry of the 38 selected stars (Table 1) with the ISOPHOT instrument (Lemke et al. 1996) on board *ISO*. Observations at 3.6, 11.5, and  $20\ \mu\text{m}$  were conducted with the P1 and P2 single-channel detectors with a

$52''$  aperture. These observations were done in staring mode (separate on-source and sky measurements). Typical on-source integration times were 32, 64, and 128 s at 3.6, 11.5, and  $20\ \mu\text{m}$ , respectively.

Photometric data were reduced with the PHOT Interactive Analysis (PIA), version 6.3.<sup>7</sup> We calibrated the data with the ISOPHOT Fine-Calibration Source 1 (FCS1). In order to improve the FCS1 calibration (presently uncertain

<sup>7</sup> PIA is a joint development by the ESA Astrophysics Division and the ISOPHOT Consortium led by the Max Planck Institute for Astronomy (MPIA), Heidelberg.

TABLE 1  
MAIN-SEQUENCE SAMPLE INFRARED PHOTOMETRY AND COLORS

OBJECT (1)	OTHER NAMES (2)	TYPE (3)	GROUND-BASED AND <i>IRAS</i>			ISOPHOT		
			$F_v$ (11.5 $\mu\text{m}$ ) (Jy) (4)	Color		$F_v$ (11.5 $\mu\text{m}$ ) (Jy) (7)	Color	
				3.6/11.5 (5)	11.5/20 (6)		3.6/11.5 (8)	11.5/20 (9)
HR 8634 .....	$\gamma$ Peg	B8 V	$1.02 \pm 0.092$	10.0	3.00	$1.108 \pm 0.061$	7.98	3.05
HR 4828 .....	$\rho$ Vir	A0 V	$0.384 \pm 0.040^a$	9.66	1.79	$0.55 \pm 0.10$	7.25	1.32
HR 6629 .....	$\gamma$ Oph	A0 V	$1.10 \pm 0.078$	8.44	2.17	$0.696 \pm 0.073$	13.7	1.41
HR 8585 .....	$\alpha$ Lac	A1 V	$0.98 \pm 0.088$	9.00	3.38	$0.77 \pm 0.12$	11.2	2.02
HR 7950 .....	$\epsilon$ Aqr	A1 V	$0.94 \pm 0.085$	9.50	3.24	$0.968 \pm 0.087$	9.25	2.85
HR 541 .....	BD Phe	A1 V	$0.204 \pm 0.025^a$	...	1.89	$0.466 \pm 0.040$	5.91	2.82
HR 4802 .....	$\tau$ Cen	A2 V	$0.99 \pm 0.17$	9.11	2.36	$0.72 \pm 0.23$	12.6	1.48
Gl 9771 .....	$\theta$ Peg	A2 V	$1.44 \pm 0.12$	8.82	3.20	$0.87 \pm 0.16$	15.6	1.75
HR 7736 .....	29 Cyg	A2 V	$0.45 \pm 0.035$	10.5	...	$0.604 \pm 0.042$	8.15	1.49
Gl 121 .....	11 Eri	A4 V	$0.983 \pm 0.092$	9.29	2.81	$1.144 \pm 0.073$	8.03	3.10
HR 269 .....	$\mu$ And	A5 V	$1.19 \pm 0.11$	9.75	2.77	$1.316 \pm 0.073$	8.96	3.07
Gl 9389 .....	$\alpha$ Crv	F0 IV–V	$1.71 \pm 0.22$	9.59	3.05	$1.114 \pm 0.063$	13.0	2.31
Gl 391 .....	...	F2 IV	$1.63 \pm 0.14$	9.39	2.76	$1.716 \pm 0.090$	9.39	2.83
HR 4167 .....	...	F4 IV	$1.60 \pm 0.14$	9.38	2.28	$0.948 \pm 0.055$	16.2	1.57
Gl 107 A .....	$\theta$ Per A	F7 V	$1.78 \pm 0.17$	10.2	3.30	$1.137 \pm 0.086$	15.2	1.48
Gl 822 A .....	...	F7 V	$1.52 \pm 0.14$	8.75	2.53	$1.551 \pm 0.086$	8.24	2.72
Gl 9706 .....	...	F8 IV	$1.46 \pm 0.13$	...	2.92	$1.251 \pm 0.082$	10.7	2.11
Gl 92 .....	$\delta$ Tri	G0.5 V	$1.56 \pm 0.15$	9.36	3.12	$1.149 \pm 0.072$	11.7	2.84
Gl 857 .....	...	G3 IV	$0.98 \pm 0.088$	8.74	2.72	$0.708 \pm 0.044$	12.4	1.52
Gl 53 A .....	$\mu$ Cas A	G5 Vb	$1.42 \pm 0.13$	9.37	3.02	$1.234 \pm 0.070$	10.6	3.23
Gl 9107 .....	$\epsilon$ For	G5 IV	$1.01 \pm 0.095$	...	3.88	$1.15 \pm 0.54$	7.43	2.49
Gl 678 .....	...	G9 IV–V	$1.02 \pm 0.096$	10.8	2.83	$0.928 \pm 0.056$	10.6	3.30
Gl 27 .....	54 Psc	K0 V	$0.721 \pm 0.068^a$	11.3	2.86	$0.829 \pm 0.049$	8.95	2.24
Gl 702 .....	70 Oph	K0 V	$5.17 \pm 0.49$	10.2	2.90	$1.90 \pm 0.14$	21.5	1.12
Gl 667 .....	...	K3 V	$1.67 \pm 0.22$	...	...	$1.12 \pm 0.25$	13.2	3.86
Gl 909 A .....	...	K3 V	$0.842 \pm 0.066^a$	...	2.98	$0.973 \pm 0.055$	8.13	2.64
Gl 879 .....	TW PsA	K4 V	$0.88 \pm 0.11$	...	2.84	$0.657 \pm 0.044$	12.1	3.15
HR 8085 .....	61 Cyg A	K5 V	$4.61^b$	$7.27^b$	$2.56^b$	$3.12 \pm 0.16$	16.0	1.66
Gl 661 .....	...	K5–M3	$0.479 \pm 0.037^a$	8.35	2.96	$0.328 \pm 0.035$	9.87	2.39
Gl 867 A .....	FK Aqr	M0 Vpe	$0.63 \pm 0.082$	6.35	2.33	$0.765 \pm 0.052$	6.61	3.18
Gl 617 A .....	...	M0 V	$0.424 \pm 0.036^{a,c}$	7.90	3.29	$0.492 \pm 0.038$	7.36	4.48
Gl 784 .....	...	M1–2 V	$0.75 \pm 0.098$	8.12	2.20	$0.481 \pm 0.048$	9.25	1.34
Gl 15 A .....	GX And	M1	$1.14 \pm 0.11$	7.34	2.38	$1.155 \pm 0.064$	7.25	2.98
Gl 809 .....	...	M0.5	$0.485 \pm 0.034^a$	9.94	3.15	$0.851 \pm 0.066$	5.62	3.72
Gl 526 .....	...	M3 V	$0.64 \pm 0.08$	9.05	1.60	$0.718 \pm 0.052$	7.42	3.10
Gl 816 .....	...	M3	...	...	...	$0.165 \pm 0.035$	10.0	0.69
Gl 644 .....	...	M3 Ve	$0.70 \pm 0.066$	8.88	3.50	$0.491 \pm 0.060$	10.7	2.27
Gl 725 A .....	...	M4	$1.10 \pm 0.10$	5.26	2.68	$0.824 \pm 0.049$	8.78	1.91

NOTE.—Col. (4) lists color-corrected *IRAS* PSC (or FSC, as noted) flux density extrapolated from  $12\ \mu\text{m}$  to the ISOPHOT 11.5 wavelength (§ 2). Cols. (5) and (6) list colors (flux ratios at the listed wavelengths in  $\mu\text{m}$ ) obtained from ground-based near-infrared ( $\sim 3.6\ \mu\text{m}$ ) photometry in Gezari et al. 1993, and from *IRAS* PSC or Faint Source Catalog (Moshir et al. 1992, FSC) 12 and  $25\ \mu\text{m}$  photometry. These data have been extrapolated to the ISOPHOT filter wavelengths (§ 2). Cols. (7)–(9) are analogous to (4)–(6), but for ISOPHOT photometry.

<sup>a</sup> *IRAS* data from the FSC.

<sup>b</sup> *IRAS* data from the Point Source Rejects Catalog (Beichman et al. 1988). The reliability of these data are uncertain, and *IRAS* colors are not plotted in Fig. 2b.

<sup>c</sup> Uncertain positional association with FSC source F16165+6721.

within a factor of  $\sim 2$ ; Habing et al. 1996) we compared our data with existing near-infrared ground-based and *IRAS* mid-infrared measurements. Near-infrared ground-based data are L-filter ( $\sim 3.5 \mu\text{m}$ ) flux densities (Gezari et al. 1993), extrapolated to  $3.59 \mu\text{m}$  (the effective  $3.6 \mu\text{m}$  ISOPHOT wavelength) along a Rayleigh-Jeans (R-J) curve. *IRAS* data are from the PSC or the Faint Source Catalog, version 2 (Moshir et al. 1992, hereafter FSC), and were color-corrected assuming a R-J spectral energy distribution (SED). *IRAS*  $12 \mu\text{m}$  data were extrapolated from  $12$  to  $11.89 \mu\text{m}$  (the effective  $11.5 \mu\text{m}$  ISOPHOT wavelength), also along an R-J curve. *IRAS*  $25 \mu\text{m}$  data were extrapolated from  $25$  to  $21.08 \mu\text{m}$  (the effective  $20 \mu\text{m}$  ISOPHOT wavelength) along the SED of a blackbody, the temperature of which was chosen to fit the PSC  $12$  and  $25 \mu\text{m}$  flux densities.

Figures 1a, 1b, and 1c show the correlation of ISOPHOT and these other measurements. We also tested the new orbit-dependent calibration in PIA version 7.0.1. The resulting correlation of our data with *IRAS* and near-infrared data was significantly worse than in Figures 1a, 1b, and 1c.

Through linear regression (Figs. 1a, 1b, and 1c), we found

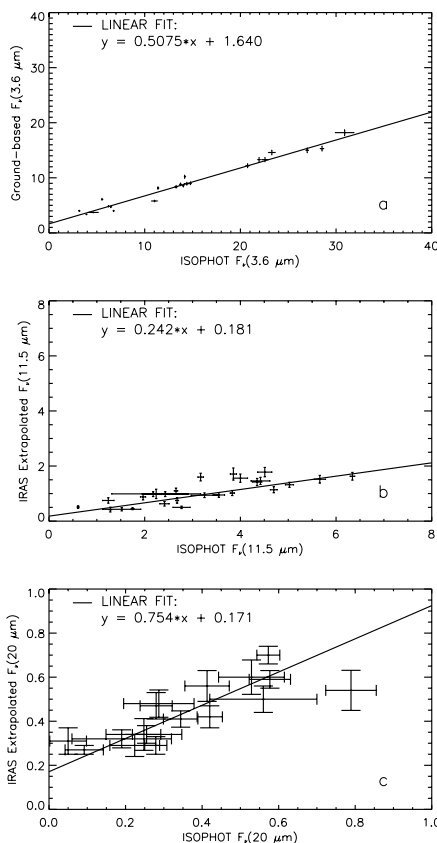


FIG. 1.—(a) Correlation of ground-based L-filter ( $\sim 3.5 \mu\text{m}$ ) flux densities (Gezari et al. 1993) against ISOPHOT  $3.6 \mu\text{m}$  flux densities. Ground-based data have been extrapolated as explained in § 2. This figure includes 22 sources from our *ISO* Key Program (Stencel & Backman 1994) of various luminosity classes, some of which are not listed in Table 1. The sources were chosen to span the flux density range in the figure. The solid line shows a linear regression fit. (b) Correlation of *IRAS* PSC or FSC and ISOPHOT flux densities at  $11.5 \mu\text{m}$ . *IRAS* data were color-corrected and extrapolated as explained in § 2. This figure includes 26 sources. (c) Correlation of *IRAS* PSC or FSC and ISOPHOT flux densities at  $20 \mu\text{m}$ . *IRAS* data were color-corrected and extrapolated (see § 2). This figure includes 17 sources.

the following transformations of ISOPHOT FCS1 staring measurements (not yet color-corrected) to ground-based and *IRAS* photometry systems. We applied these transformations to the ISOPHOT flux densities of the stars in Table 1:

$$F'_{\nu}(3.6 \mu\text{m}) = (0.5075 \pm 0.0077)F_{\nu}(3.6 \mu\text{m}) + (1.640 \pm 0.076) \text{ Jy} \quad \text{for } 3 \text{ Jy} < F_{\nu}(3.6 \mu\text{m}) < 30 \text{ Jy}; \quad (1)$$

$$F'_{\nu}(11.5 \mu\text{m}) = (0.242 \pm 0.013)F_{\nu}(11.5 \mu\text{m}) + (0.181 \pm 0.034) \text{ Jy} \quad \text{for } 1 \text{ Jy} < F_{\nu}(11.5 \mu\text{m}) < 8 \text{ Jy}; \quad (2)$$

$$F'_{\nu}(20 \mu\text{m}) = (0.754 \pm 0.091)F_{\nu}(20 \mu\text{m}) + (0.171 \pm 0.034) \text{ Jy} \quad \text{for } 0.1 \text{ Jy} < F_{\nu}(20 \mu\text{m}) < 1 \text{ Jy}. \quad (3)$$

We believe that these transformations can improve the calibration of similar staring ISOPHOT data in other observers' programs. They will also yield insights toward eventually establishing the ISOPHOT calibration. Our observations can be combined with future ground-based photometry, particularly at  $10$  and  $20 \mu\text{m}$ , to further refine the ISOPHOT calibration.

### 3. ANALYSIS OF ISOPHOT PHOTOMETRY

#### 3.1. Color-Color Diagrams of ISOPHOT, *IRAS*, and Ground-based Photometry

In order to detect infrared excesses in the SEDs of the sources in Table 1, we plotted color-color diagrams of their infrared flux densities. Figure 2a is the color-color diagram of ISOPHOT  $11.5 \mu\text{m}/20 \mu\text{m}$  against  $3.6 \mu\text{m}/11.5 \mu\text{m}$  flux densities of the stars in Table 1. Figure 2b is a similar color-color diagram of available ground-based L-filter flux densities (Gezari et al. 1993) and *IRAS* PSC or FSC  $12$  and  $25 \mu\text{m}$  flux densities. These data have been extrapolated to the ISOPHOT filter effective wavelengths, and *IRAS* data have been color-corrected as explained in § 2. Figure 2a includes data for 38 stars, and Figure 2b for 29 stars with available measurements. Figures 2a and 2b also indicate the locus of blackbody colors (dashed line) for temperatures ranging from  $3000 \text{ K}$  to infinity (R-J limit). This locus thus encompasses typical photospheric temperatures of main-sequence stars. In Figures 2a and 2b we also include the colors of  $\alpha$  Lyr (from data in Wamsteker 1981, Rieke, Lebofsky, & Low 1985, and/or Hanner & Tokunaga 1991). The comparison of infrared colors of  $\alpha$  Lyr (the prototypical main-sequence star with an infrared excess; Aumann et al. 1984) with infrared colors of main-sequence photospheres and those measured for our sources allows us to detect excesses and understand their nature. We tentatively identified sources with excesses in their ISOPHOT SEDs if their  $3.6/11.5$  and  $11.5/20$  colors deviated by more than 1 standard deviation ( $\sigma$ ) from the colors expected for stellar photospheres as defined by the dashed line in Figure 2a. This technique resembles that employed by Mannings & Barlow (1998) in their search for *IRAS* excesses. We later checked the reality of ISOPHOT excesses by comparing them with *IRAS* SED results, as explained in § 3.2. Table 2 indicates whether mid-infrared excesses for our sources are detected (Y/N) in *IRAS* (cols. [2] and [3]) and tentatively in ISOPHOT (cols. [4] and [5]) observations, relative to photospheric continua fit at  $3.6 \mu\text{m}$ . Entries in Table 2 marked with a question mark

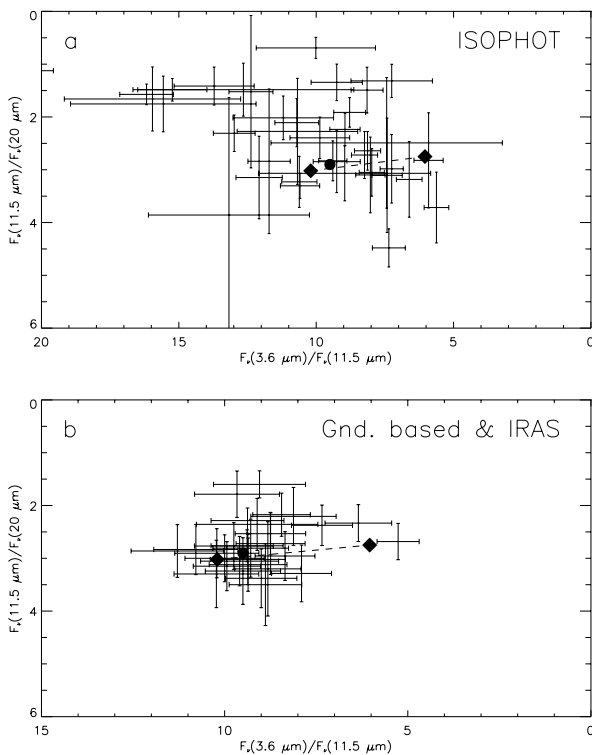


FIG. 2.—(a) Color-color diagram (11.5/20 against 3.6/11.5) of ISOPHOT flux densities transformed by means of eqs. (1)–(3). Error bars are 1 standard deviation in the flux density ratios. The dashed line represents the colors of blackbodies whose temperatures range from infinity or R-J limit (filled diamond at left end of dashed line) down to 3000 K (filled diamond at right). The filled circle represents the colors of  $\alpha$  Lyr. (b) Same as (a), but 3.6  $\mu$ m data are from Gezari et al. (1993), and 11.5 and 20  $\mu$ m data are from the *IRAS* PSC or FSC. These data were extrapolated as explained in the text (§ 2).

mean statistically insignificant excesses, which can be regarded as nondetections in the rest of our arguments.

If near-infrared photometry was not available for stars with *IRAS* 12 and 25  $\mu$ m measurements, we estimated whether 12  $\mu$ m excesses were present from their *V* magnitudes and photospheric  $V - [12]$  relations (Waters, Coté, & Aumann 1987; Jaschek et al. 1991; Mathioudakis & Doyle 1993). Stars for which these estimates were made are indicated in Table 1 by ellipses in column (5), and by a nonblank entry (N in all such cases, because we did not detect *IRAS* 12  $\mu$ m excesses in this way) in Table 2, column (2). Three of our sources (29 Cyg, Gl 667, and Gl 816) have only upper limits in at least one of the 12 and 25  $\mu$ m *IRAS* measurements, indicated by ellipses in Table 2, columns (2) and (3), respectively. The colors of these stars and those of stars without near-infrared photometry cannot be plotted in Figure 2b. In addition, we did not plot the colors of 61 Cyg A, because its *IRAS* photometry is from the Point Source Rejects Catalog (Beichman et al. 1988). The binary separation of the two nearly equally bright components, A and B, of 61 Cyg is around the *IRAS* diffraction limit. Consequently, the *IRAS* flux extraction process for 61 Cyg A *IRAS* data are questionable.

### 3.2. Statistical Revision of ISOPHOT SEDs and Excesses

In order to interpret the apparent excesses and other deviations from photospheric SEDs tentatively indicated by

our ISOPHOT photometry, we compared them to the results from *IRAS* photometry listed in Table 2.

We found that the ISOPHOT colors of  $\sim 26\%$  of our sources (10 stars, listed in Table 3), often our fainter targets, do not indicate the same results (Table 2, cols. [4] and [5]) as those from *IRAS* colors (Table 2, cols. [2] and [3]) regarding the presence (Y) or absence (N) of excesses at 11.5 or 20  $\mu$ m. The average color-corrected *IRAS* 11.5  $\mu$ m flux density [ $F_{\nu}(11.5 \mu\text{m})$ ] of these sources (Table 1, col. [4]) is  $0.81 \pm 0.15$  Jy. The average *IRAS*  $F_{\nu}(11.5 \mu\text{m})$  of the rest of our sources, whose ISOPHOT and *IRAS* photometry indicate the same excesses or absences thereof at 11.5 or 20  $\mu$ m, is  $1.46 \pm 0.24$  Jy. Thus, the former sources are on average fainter than the latter. In fact, of the seven stars in Table 1 with *IRAS* FSC photometry ( $\rho$  Vir, BD Phe, 54 Psc, Gl 909 A, Gl 661, Gl 617 A, and Gl 809), five have discrepant ISOPHOT and *IRAS* results for the presence or absence of excesses at 11.5 or 20  $\mu$ m (Tables 2 and 3), thus illustrating that these sources tend to be faint. We believe that for these faint sources the 11.5 and 20  $\mu$ m ISOPHOT transformations (eqs. [2] and [3]) are not entirely correct. A larger number of data points in Figures 1b and 1c for faint stars would be needed to refine the transformation for 11.5  $\mu$ m flux densities lower than  $\sim 1$  Jy.

The ISOPHOT results for 11.5 or 20  $\mu$ m excesses or the lack thereof that are discrepant with respect to *IRAS*, and referred to above, are listed in Table 3. In Table 3 we also list references to previous *IRAS* detections of excesses in our sources that confirm our technique used in Figure 2b. (We do not list references in Table 3 for previous nondetections of *IRAS* excesses.) The ISOPHOT results in Table 3 are highly questionable and require future confirming observations. Of these sources, Table 2, column (6), lists Gl 809 as showing an “*ISO* 11.5 anomaly,” meaning that its ISOPHOT  $F_{\nu}(11.5 \mu\text{m})$  is overestimated with respect to both 3.6 and 20  $\mu$ m. We do not believe in the physical reality of the 11.5  $\mu$ m anomaly, because an excess at 11.5  $\mu$ m and not at 20  $\mu$ m would imply a much narrower emission band than the SED from one or more blackbodies or any other main-sequence circumstellar dust emission feature ever seen (BP93). Table 2, column (6), also lists Gl 617 A as having an “*ISO* 20  $\mu$ m anomaly,” meaning that its ISOPHOT  $F_{\nu}(20 \mu\text{m})$  is underestimated with respect to 11.5  $\mu$ m (and 3.6  $\mu$ m). The 20  $\mu$ m anomaly cannot be real, because the 11.5/20 (and 3.6/20) colors would imply an SED substantially steeper than R-J. The star  $\epsilon$  For exhibits a similar *IRAS* 20  $\mu$ m anomaly (Table 2, col. [6]) in the same sense as above, which we also regard as unphysical.

Figure 2a and Table 2, column (6), show that 26% of our sources (10 stars) have ISOPHOT 3.6/11.5 colors apparently steeper than R-J colors, referred to as “*ISO* 3.6 anomalies.” The colors of these sources appear in the leftmost portion of Figure 2a. It is not likely that the ISOPHOT 11.5  $\mu$ m fluxes of these sources are deficient with respect to photospheric SEDs. Instead, their ISOPHOT 3.6  $\mu$ m fluxes are overestimated, even after the transformation in equation (1). We think that this is the case because the ISOPHOT 3.6/20 colors of these sources also tend to be steeper than R-J colors. In addition, only one of these sources,  $\gamma$  Oph, and perhaps also 70 Oph, exhibits a 20  $\mu$ m excess; many more of these sources would show apparent 20  $\mu$ m excesses (seen as small 11.5/20 colors in Fig. 2a) if their transformed 11.5  $\mu$ m ISOPHOT fluxes were deficient. The ISOPHOT and *IRAS* results for the presence or absence of excesses at

TABLE 2  
 MAIN-SEQUENCE SAMPLE INFRARED EXCESSES (*IRAS*) AND TENTATIVE EXCESSES (*ISOPHOT*)

NAME (1)	GROUND-BASED AND <i>IRAS</i> EXCESS		<i>ISOPHOT</i> TENTATIVE EXCESS		SED Anomaly (6)
	11.5 (2)	20 (3)	11.5 (4)	20 (5)	
$\gamma$ Peg .....	N	N	N	N	...
$\rho$ Vir .....	N	Y	Y	Y	...
$\gamma$ Oph .....	N	Y	N	Y	ISO 3.6
$\alpha$ Lac .....	N	N	N	Y	...
$\epsilon$ Aqr .....	N	N	N	N	...
BD Phe .....	N	Y	Y	N	...
$\tau$ Cen .....	N	Y	N	Y	...
$\theta$ Peg .....	N	N	N	N	ISO 3.6
29 Cyg .....	N	...	N	Y	...
11 Eri .....	N	N	N	N	...
$\mu$ And .....	N	N	N	N	...
$\alpha$ Crv .....	N	N	N	N	ISO 3.6
Gl 391 .....	N	N	N	N	...
HR 4167 .....	N	Y	N	N	ISO 3.6
$\theta$ Per A .....	N	N	N	N	ISO 3.6
Gl 822 A .....	N	Y	N	N	...
Gl 9706 .....	N	N	N	N	...
$\delta$ Tri .....	N	N	N	N	ISO 3.6
Gl 857 .....	N	N	N	N	ISO 3.6
$\mu$ Cas A .....	N	N	N	N	...
$\epsilon$ For .....	N	N	N	N	IRAS 20
Gl 678 .....	N	N	N	N	...
54 Psc .....	N	N	N	Y	NIR 3.6
70 Oph .....	N	N	N	?	ISO 3.6
Gl 667 .....	N	...	N	N	...
Gl 909 A .....	N	N	N	N	...
TW PsA .....	N	N	N	N	ISO 3.6
61 Cyg A .....	N	N	N	N	ISO 3.6
Gl 661 .....	N	N	N	N	...
FK Aqr .....	N	?	?	N	...
Gl 617 A .....	N	N	?	N	ISO 20
Gl 784 .....	N	Y	N	Y	...
GX And .....	N	?	N	N	...
Gl 809 .....	N	N	N	N	NIR 3.6, ISO 11.5
Gl 526 .....	N	Y	N	N	...
Gl 816 .....	...	...	N	Y	...
Gl 644 .....	N	N	N	N	...
Gl 725 A .....	N	N	N	Y	...

NOTE.—Cols. (2) and (3) indicate whether excess emission exists (Y/N) in *IRAS* photometry at the listed wavelengths (as in Table 1), relative to a photospheric fit at ground-based 3.6  $\mu$ m photometry. Entries marked with a question mark mean statistically insignificant excesses. Cols. (4) and (5) indicate whether excess emission tentatively exists in *ISOPHOT* photometry, analogously to cols. (2) and (3), relative to photospheric fits at *ISOPHOT* 3.6  $\mu$ m photometry. Results in cols. (4) and (5) are subject to confirmation by comparison with *IRAS* (§ 3.2). The term “SED anomaly” in col. (6) is used to indicate *ISOPHOT* (*ISO*), *IRAS*, or ground-based near-infrared (NIR) photometry data that are overestimated at 3.6 or 11.5  $\mu$ m, or underestimated at 20  $\mu$ m. These overestimates or underestimates cannot be regarded as plausibly physical, as explained in § 3.2.

11.5 and 20  $\mu$ m are discrepant for only one of these sources (HR 4167; see Table 3), thus further suggesting that the apparent *ISOPHOT* anomaly in most of them occurs not at 11.5 or 20  $\mu$ m, but at 3.6  $\mu$ m. The average *ISOPHOT*  $F_{\nu}(3.6 \mu\text{m})$  of these 10 stars, computed from Table 1, columns (4) and (5), is  $19 \pm 4.4$  Jy, whereas the average for the rest of our sources is  $8.2 \pm 0.72$  Jy. Thus, the sources with *ISOPHOT* 3.6  $\mu$ m anomalies are on the average brighter than those without such anomalies. We believe that our linear transformation (eq. [1]) is not entirely correct for bright 3.6  $\mu$ m sources. An improved regression in Figure 1a might have a shallower slope for large  $F_{\nu}(3.6 \mu\text{m})$ . The

improved relation could be established with more data points in Figure 1a with  $F_{\nu}(3.6 \mu\text{m}) \gtrsim 20$  Jy. The stars 54 Psc and Gl 809 exhibit similar near-infrared (NIR) 3.6  $\mu$ m anomalies, meaning that their ground-based near-infrared flux densities are overestimated in the same sense as above. However, none of the *ISO* anomalies are matched with the same wavelength (NIR) or *IRAS* anomalies.

Apart from the instances of anomalies described above, we found that the *ISOPHOT* colors of  $\sim 74\%$  of our sources (28 stars) in Table 1 support the same results as *IRAS* colors regarding the presence or absence of 11.5 or 20  $\mu$ m excess (Table 2). These results are listed in Table 4.

TABLE 3  
ISOPHOT SED RESULTS NOT CONFIRMED BY *IRAS*

Name	Reference for <i>IRAS</i> Excess	ISOPHOT SED Result
$\rho$ Vir .....	...	11.5 $\mu\text{m}$ excess
$\alpha$ Lac .....	...	20 $\mu\text{m}$ excess
BD Phe .....	1	11.5 $\mu\text{m}$ excess; nondetection of <i>IRAS</i> 20 $\mu\text{m}$ excess
HR 4167 .....	1	nondetection of <i>IRAS</i> 20 $\mu\text{m}$ excess
Gl 822 A.....	2	nondetection of <i>IRAS</i> 20 $\mu\text{m}$ excess
54 Psc .....	...	20 $\mu\text{m}$ excess
Gl 526 .....	...	nondetection of <i>IRAS</i> 20 $\mu\text{m}$ excess
Gl 725 A.....	...	20 $\mu\text{m}$ excess
Gl 617 A.....	...	<i>ISO</i> 20 $\mu\text{m}$ SED anomaly <sup>a</sup>
GL 809 .....	...	<i>ISO</i> 11.5 $\mu\text{m}$ SED anomaly <sup>a</sup>

<sup>a</sup> The term “SED anomaly” is used to indicate ISOPHOT (*ISO*), *IRAS*, or ground-based NIR photometry data that are overestimated at 3.6 or 11.5  $\mu\text{m}$ , or underestimated at 20  $\mu\text{m}$ . These overestimates or underestimates cannot be regarded as plausibly physical, as explained in § 3.2.

REFERENCES.—(1) *IRAS* excess reported for the first time here; (2) Backman & Gillett 1987. We do not list references for photospheric *IRAS* SED results.

References to previous *IRAS* detections of excesses are also listed in the notes to Table 4, but nondetections of *IRAS* excesses are not. We are confident in the physical reality of these ISOPHOT results because of the confirmation by *IRAS*. In this group of sources,  $\sim 86\%$  (24 stars) have photospheric SEDs (considering the anomaly cases as observational artifacts). None show 11.5  $\mu\text{m}$  excesses, and  $\sim 14\%$  (four stars) show 20  $\mu\text{m}$  excesses. Small excess emission at 20  $\mu\text{m}$ , without any shorter wavelength excesses, such as in the latter four sources, could imply that such systems have relatively cool ( $T \sim 100$  K) circumstellar dust. These systems might thus be similar to  $\alpha$  Lyr.

The above statistics, from a subset of our sample of stars, can be compared to those from all of our sources with *IRAS* measurements (37 stars). The two stars in this sample that have only *IRAS* upper limits at  $\sim 20$   $\mu\text{m}$  (29 Cyg and Gl 667) can be regarded as not having detectable 20  $\mu\text{m}$  excesses. The *IRAS* statistics of this set then show that  $\sim 76\%$  (29 stars) have photospheric SEDs (regarding the

three anomalies in Table 2 as artifacts); none have 11.5  $\mu\text{m}$  excesses, and  $\sim 22\%$  (eight stars) have  $\sim 20$   $\mu\text{m}$  excesses. There is a larger proportion of *IRAS* 20  $\mu\text{m}$  excess detections in this sample than in the previous one (Table 4). We think that the larger *IRAS* beam ( $45'' \times 279''$  at 25  $\mu\text{m}$ , relative to our 52'' ISOPHOT aperture) yields more detections of 20  $\mu\text{m}$  emission from background sources.

For comparison, the ISOPHOT statistics of this same set of 37 sources show that  $\sim 76\%$  (28 stars) have photospheric SEDs; 5% (two stars) have 11.5  $\mu\text{m}$  excesses, and  $\sim 21\%$  (eight stars) have 20  $\mu\text{m}$  excesses. However, we recall that about one-fourth of these sources have anomalous 3.6  $\mu\text{m}$  flux densities, and about one-fourth of the 37 stars have SEDs derived from ISOPHOT that are discrepant with SEDs derived from *IRAS* and ground-based data. Therefore, the above ISOPHOT statistics of this set are inconclusive, even though the fraction of 20  $\mu\text{m}$  excesses appears to resemble that of the *IRAS* statistics.

We also obtained ISOPHOT SED results for three stars that have no *IRAS* measurements (at best only upper limits). These are Gl 816 (20  $\mu\text{m}$  excess), 29 Cyg (20  $\mu\text{m}$  excess), and Gl 667 (photospheric 20  $\mu\text{m}$  SED). These results cannot be confirmed or ruled out by *IRAS*, but may be by future observations.

### 3.3. Models of Vega-Type Dust Excesses

We modeled the detected ISOPHOT excesses with single-temperature blackbody emission. These preliminary models let us estimate the approximate location and temperature of circumstellar dust. We will consider more complex models with multitemperature grain distributions when far-infrared ISOPHOT data are reliably calibrated, and when higher spectral resolution measurements are obtained. We computed these models for all of our sources that showed ISOPHOT 11.5 or 20  $\mu\text{m}$  excesses, even though some of these results (see Table 3 and end of § 3.2) are only tentative at this point. Table 5 lists the single-temperature model results. The quantity  $T_{\text{dust}}$  was determined from model fits to the observed 11.5 (tentative) and/or 20  $\mu\text{m}$  excess flux densities. We estimated an uncertainty up to 10% in  $T_{\text{dust}}$ . Figure 3 illustrates a model fit to the photometry of  $\rho$  Vir. This model is a compromise fit to ISOPHOT and *IRAS* photometry. The 11.5 and 20  $\mu\text{m}$

TABLE 4  
ISOPHOT SED RESULTS CONFIRMED BY *IRAS*:  
LIST OF SOURCES

20 $\mu\text{m}$ Excesses			
$\rho$ Vir <sup>a</sup>	$\gamma$ Oph <sup>b,c</sup>	$\tau$ Cen <sup>d</sup>	Gl 784 <sup>e</sup>
Photospheric 11.5 and 20 $\mu\text{m}$ Flux Densities			
$\gamma$ Peg	$\epsilon$ Aqr	$\theta$ Peg	11 Eri
$\mu$ And	$\alpha$ Crv	Gl 391	$\theta$ Per A
Gl 9706	$\delta$ Tri	Gl 857	$\mu$ Cas A
$\epsilon$ For	Gl 678	70 Oph	Gl 909 A
TW PsA	61 Cyg A	Gl 661	FK Aqr
Gl 617 A	GX And	GL 809	Gl 644

NOTE.—These results are apart from *ISO*, *IRAS*, or NIR anomalies, as defined in the notes to Table 2 and § 3.2. References to previous *IRAS* excess detections are given below. As in Table 3, we do not give references to photospheric *IRAS* SED results.

<sup>a</sup> Cheng et al. 1992.

<sup>b</sup> Coté 1987.

<sup>c</sup> Sadakane & Nishida 1986.

<sup>d</sup> *IRAS* excess reported for the first time here.

<sup>e</sup> Mathioudakis & Doyle 1993.

TABLE 5  
SINGLE-TEMPERATURE BLACKBODY MODELS OF  
ISOPHOT EXCESSES

Name (1)	$T_{\text{dust}}$ (K) (2)	$r_{\text{dust}}$ (AU) (3)	$\tau$ (4)
$\rho$ Vir <sup>a</sup> .....	190	14	$5 \times 10^{-5}$
$\gamma$ Oph .....	100	58	$2 \times 10^{-6}$
$\alpha$ Lac <sup>a</sup> .....	130	34	$1 \times 10^{-6}$
BD Phe <sup>a</sup> .....	225	11	$5 \times 10^{-5}$
$\tau$ Cen .....	130	33	$8 \times 10^{-6}$
29 Cyg <sup>b</sup> .....	150	25	$1 \times 10^{-5}$
54 Psc <sup>a</sup> .....	150	2.1	$2 \times 10^{-5}$
Gl 784 .....	105	1.3	$9 \times 10^{-5}$
Gl 816 <sup>b</sup> .....	120	0.40	$4 \times 10^{-4}$
Gl 725 A .....	150	0.25	$2 \times 10^{-4}$

NOTE.—Col. (2) lists the temperature,  $T_{\text{dust}}$ , of single-temperature blackbody dust models fitted to the excess flux densities observed with ISOPHOT at 11.5 and/or 20  $\mu\text{m}$ . Col. (3) lists the radiative equilibrium distance,  $r_{\text{dust}}$ , from the star for blackbody grains at temperature  $T_{\text{dust}}$ . Col. (4) is the fractional dust luminosity  $\tau$ , or the ratio of integrated excess emission from dust to integrated photospheric emission. See text for the computation of  $\tau$ .

<sup>a</sup> ISOPHOT SEDs are discrepant with respect to *IRAS* measurements, and thus these excesses are questionable (see Table 3).

<sup>b</sup> ISOPHOT SEDs are presented in the absence of reliable *IRAS* data, and thus cannot be confirmed or ruled out.

ISOPHOT flux densities are higher than *IRAS*, and the 11.5  $\mu\text{m}$  ISOPHOT apparent excess is not confirmed by *IRAS*. The model results for  $\rho$  Vir are thus only tentative at this point, as are those of other sources in Table 5 with discrepant ISOPHOT and *IRAS* data. The quantity  $r_{\text{dust}}$  in all models is the radiative equilibrium distance of blackbody grains from the star, at temperature  $T_{\text{dust}}$ . The uncertainty in  $r_{\text{dust}}$ , derived from those in  $T_{\text{dust}}$ , stellar radius, and effective photospheric temperature (see below for the latter

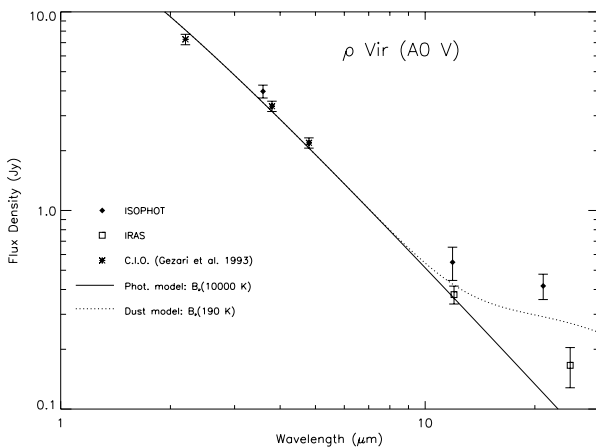


FIG. 3.—SED of  $\rho$  Vir, obtained from transformed 3.6, 11.5, and 20  $\mu\text{m}$  ISOPHOT flux densities (filled diamonds), *IRAS* FSC color-corrected (assuming a R-J SED) 12 and 25  $\mu\text{m}$  flux densities (open squares), and KLM photometry from Gezari et al. 1993 (asterisks). The solid line shows a  $10^4$  K photospheric blackbody SED fitted by eye to the KLM flux densities. The dotted line shows a 190 K blackbody SED that models the excess emission from dust around  $\rho$  Vir. This model is a compromise fit to the ISOPHOT and *IRAS*  $\sim 12$  and 20–25  $\mu\text{m}$  data.

two) is roughly 50%. Table 5 also lists the fractional dust luminosity  $\tau$  of the systems, defined as the ratio of integrated excess flux emitted from dust,  $\int_0^\infty dv F_\nu(\text{dust})$ , to the integrated flux emitted from the star alone in the absence of circumstellar material,  $\int_0^\infty dv F_\nu(\text{phot})$ . We estimated the latter integrated flux simply as  $\sigma T_*^4 \Omega_*$ , where  $\sigma$  is the Stefan-Boltzmann constant divided by  $\pi$ ,  $T_*$  is the effective photospheric temperature for the star's spectral type (Allen 1973), and  $\Omega_*$  is the solid angle subtended by the star. Typical uncertainties in  $T_*$  and stellar radii (the latter also from Allen 1973, and needed in the computation of  $r_{\text{dust}}$ ) are  $\pm 250$  K and  $\sim 10\%$ , respectively, estimated by comparing Allen's values with those from more recent calibrations of effective photospheric temperatures (Gray & Corbally 1994), or those derived from optical measurements by Malagnini & Morossi (1990). The solid angle  $\Omega_*$  is determined from the normalization of photospheric flux density to that observed at 3.6  $\mu\text{m}$ . The integrated excess flux from dust is obtained by using  $F_\nu(\text{dust}) = B_\nu(T_{\text{dust}})\Omega_{\text{dust}}$ , where  $B_\nu(T_{\text{dust}})$  is the Planck function, and where  $\Omega_{\text{dust}}$  is determined from the normalization of excess flux density to that observed in the mid-infrared with ISOPHOT. We integrated  $F_\nu(\text{dust})$  from the near-infrared to 20 or 25  $\mu\text{m}$  (if *IRAS* 25  $\mu\text{m}$  data was available). Far-infrared (e.g., 60  $\mu\text{m}$ ) data are not yet available, and thus our dust fractional luminosities are lower limits. However, our values of  $\tau$  represent a significant fraction of the actual ones, because the integrals of  $F_\nu(\text{dust})$  over frequency have higher contributions at higher frequencies (in the near-infrared) than in the far-infrared. The uncertainties in  $\tau$  are roughly 30%.

Our ISOPHOT survey yielded detections of systems with fractional dust luminosities  $\tau$  ranging from  $1 \times 10^{-6}$  to  $4 \times 10^{-4}$ . Thus, these excesses are small or moderate (and some are only tentative at this point). For comparison, only 25% of A-type main-sequence stars have  $\tau > 5 \times 10^{-6}$  (Backman & Gillett 1987). It is significant that three of our sources (Gl 784, Gl 816, and Gl 725 A) have  $\tau \sim 10^{-4}$ . These sources, with the largest fractional dust luminosities in our sample, are all of spectral type M.

Other M-type main-sequence stars with previously known *IRAS* excesses are Gl 447 (= Ross 128 = FI Vir, Backman, Gillett, & Low 1986), CC Eri (Mannings & Barlow 1998), Gl 644 (*IRAS* excess longward of 25  $\mu\text{m}$  and thus not reported in our Table 4, Mathioudakis & Doyle 1993), Gl 803 (= AU Mic, Mathioudakis & Doyle), and Gl 285 (= YZ CMi, Mullan et al. 1992). The infrared excesses of Gl 644 and Gl 285 are known to be from free-free emission in stellar winds.

Table 5 indicates that six of our sources have dust material at distances of less than 15 AU from the stars. Of these,  $\rho$  Vir and BD Phe have very warm dust ( $T \geq 200$  K) around them. The dust around these six sources is within the plausible planetary region of these systems. If planets or protoplanets are present, they could affect the dust region structure in ways that could be observed through imaging observations. In contrast, Table 5 indicates that  $\gamma$  Oph has much cooler material at 100 K and located beyond 40 AU from the star. This source possibly has an inner hole in its dust region (as inferred also by Fajardo-Acosta et al. 1998 from ground-based and *IRAS* photometry), and we might thus be seeing only the “Kuiper Belt” of this system. Table 5 lists three other stars ( $\alpha$  Lac,  $\tau$  Cen, and 29 Cyg) with dust at 130–150 K and located at 25–34 AU. This dust could represent both planetary and Kuiper Belt regions material.

Whether the Kuiper Belt regions of these systems imply planetary formation or failed planetary systems remains an exciting area of future research.

We gratefully acknowledge partial support for this effort from NASA *ISO* Key Project grant NAG5-3411 and JPL

grant 961503 to the University of Denver. We also thank George Helou, Michael Bica, Deborah Levine, Nanyao Lu, Ann Wehrle, Martin Haas, and the IPAC and *ISO* ESTEC staff for assistance in conducting this study. The research has made use of the SIMBAD database, operated at CDS, Strasbourg, France.

## REFERENCES

- Allen, C. W. 1973, *Astrophysical Quantities* (London: Athlone)
- Aumann, H. H., Gillett, F. C., Beichman, C. A., de Jong, T., Houck, J. R., Low, F. J., Neugebauer, G., Walker, R. G., & Wesselius, P. R. 1984, *ApJ*, 278, L23
- Aumann, H. H., & Probst, R. G. 1991, *ApJ*, 368, 264
- Backman, D. E. 1998, in *Exozodiacal Dust Workshop*, ed. D. E. Backman, L. J. Caroff, S. A. Sandford, & D. H. Wooden (NASA CP 1998-10155) (Moffett Field: NASA Ames), 107
- Backman, D. E., & Gillett, F. C. 1987, in *Cool Stars, Stellar Systems, and the Sun*, ed. J. L. Linsky & R. E. Stencel (Berlin: Springer), 340
- Backman, D. E., Gillett, F. C., & Low, F. J. 1986, *Adv. Space Res.*, 6, 43
- Backman, D. E., & Paresce, F. 1993, in *Protostars and Planets III*, ed. E. H. Levy, J. I. Lunine, & M. S. Mathews (Tucson: Univ. Arizona Press), 1253 (BP93)
- Beichman, C. A., Neugebauer, G., Habing, H. J., Clegg, P. E., & Chester, T. J., ed. 1988, *IRAS Catalogs and Atlases: Explanatory Supplement* (Washington: GPO)
- Burrows, C. J., Krist, J. E., Stapelfeldt, K. R., & WFPC2 Investigation Definition Team. 1995, *BAAS*, 27, 32.05
- Cheng, K.-P., Bruhweiler, F. C., Kondo, Y., & Grady, C. A. 1992, *ApJ*, 396, L83
- Coté, J. 1987, *A&A*, 181, 77
- Dominik, C., & HJHVEGA Consortium. 1998, *Ap&SS*, 255, 103
- Fajardo-Acosta, S. B., Telesco, C. M., & Knacke, R. F. 1998, *AJ*, 115, 2101
- Gezari, D. Y., Schmitz, M., Pitts, P. S., & Mead, J. L. 1993, *Catalog of Infrared Observations* (NASA RP-1294) (Washington: GPO)
- Gliese, W. 1969, *Catalog of Nearby Stars* (Heidelberg: Veröfentl. Astron. Rechen-Instituts), 22
- Gliese, W., & Jahreiss, H. 1979, *A&AS*, 38, 423
- Gray, R. O., & Corbally, C. J. 1994, *AJ*, 107, 742
- Habing, H. J., et al. 1996, *A&A*, 315, L233
- Hanner, M. S., & Tokunaga, A. T. 1991, in *Comets in the Post-Halley Era*, Vol. 1, ed. R. L. Newburn et al. (Dordrecht: Kluwer), 67
- Heap, S. R., Lindler, D. J., Woodgate, B., & STIS ID Team. 1997, *BAAS*, 29, 1285
- Hoffleit, D., & Jaschek, C. 1982, *The Bright Star Catalog* (New Haven: Yale Univ. Obs.)
- Jaschek, C., Jaschek, M., Andriolat, Y., & Egret, D. 1991, *A&A*, 252, 229
- Jenkins, L. F. 1963, *General Catalog of Trigonometric Stellar Parallaxes* (New Haven: Yale Univ. Obs.)
- Joint IRAS Science Working Group. 1988, *IRAS Point Source Catalog, Version 2* (Washington: GPO) (PSC)
- Kessler, M. F., et al. 1996, *A&A*, 315, L27
- Knacke, R. F., Fajardo-Acosta, S. B., Telesco, C. M., Hackwell, J. A., Lynch, D. K., & Russell, R. W. 1993, *ApJ*, 418, 440
- Lagage, P. O., & Pantin, E. 1994, *Nature*, 369, 628
- Lemke, D., et al. 1996, *A&A*, 315, L64
- Malagnini, M. L., & Morossi, C. 1990, *A&AS*, 85, 1015
- Mannings, V., & Barlow, M. J. 1998, *ApJ*, 497, 330
- Mathioudakis, M., & Doyle, J. G. 1993, *A&A*, 280, 181
- Moshir, M., et al. 1992, *Explanatory Supplement to the IRAS Faint Source Survey, Version 2* (JPL D-10015 8/92) (Pasadena: Jet Propulsion Laboratory) (FSC)
- Mullan, D. J., Doyle, J. G., Redman, R. O., & Mathioudakis, M. 1992, *ApJ*, 397, 225
- Plets, H. 1997, Ph.D. thesis, Katholieke Univ. Leuven
- Rieke, G. H., Lebofsky, M. J., & Low, F. J. 1985, *AJ*, 90, 900
- Sadakane, K., & Nishida, M. 1986, *PASP*, 98, 685
- Stencel, R. E., & Backman, D. E. 1994, *Ap&SS*, 212, 417
- Tremaine, S. 1990, in *Baryonic Dark Matter*, ed. D. Lyndell-Bell & G. Gilmore (Dordrecht: Kluwer), 37
- Wamsteker, W. 1981, *A&A*, 97, 329
- Waters, L. B. F. M., Cote, J., & Aumann, H. H. 1987, *A&A*, 172, 225